

Symmetry-breaking polygons on a rotating fluid surface

Christopher Ong Xianbo
World Scientific Publishing Company, Singapore

Abstract: When a circular plate is rotated at the bottom of a cylindrical vessel containing fluid, the fluid surface can form stable polygons under certain conditions. This phenomenon is very surprising, as it seems that the rotational symmetry of the setup is mysteriously broken when polygons are formed. I experimentally measured the geometries of the formed polygons and studied their dependence on parameters such as the plate rotational rate. Both the number of sides and the sizes of the polygons were found to increase when the plate rotated faster.

In my research, I sought to develop a theoretical model that could accurately predict the properties of the formed polygons in agreement with experimental results. Taking on a novel approach of analysing the forces on a fluid particle travelling along the boundary of the polygon, the mechanism of polygon formation and the effect of the plate rotation on the polygons were physically understood. Applying it quantitatively, with considerations on the properties of the fluid flow, a differential equation governing the polygon's steady-state geometry was formulated. A high degree of predictive power into the shape of the polygon was achieved, closely matching experimental data.

1 Introduction

When a plate is rotated at the bottom of a cylindrical vessel that is partially filled with fluid, the surface of the fluid surprisingly forms polygons under certain conditions, breaking rotational symmetry. These polygons tend to be stable, and they rotate in the same direction as the plate but at a lower rate. Prior studies have investigated the number of sides of the polygons formed; Jansson et al. (2006) experimentally tested the dependence of the number of sides of the polygons on parameters like plate rotation and fluid volume, while Tophøj et al. (2013) theorised the polygon formation to be a result of resonance between gravity waves and centrifugal waves and used this principle to predict the number of sides of polygons. Due to the complex nature of the fluid flow in the setup, less investigation has gone into predicting the geometry of the polygons' shapes. Moreover, a physical account of the phenomenon and its dependence on variables remain less well-understood.

This study developed a quantitative model of the shapes of polygons formed under this phenomenon. This was built on a force analysis of surface fluid particles, which circumvented the need to fully solve for the complicated flow profile of the fluid. Simultaneously, this provided qualitative insight into the polygon formation and the dependence of its properties on parameters like plate angular velocity and fluid volume.

2 Method

A thin circular acrylic plate was placed near the bottom of a transparent cylindrical vessel, both with approximately equal radii $R = 8.65\text{cm}$. The plate was attached to a vertical axle below, which passed through the base of the vessel via a waterproof bearing and was rotated at a controllable angular velocity ω by LEGO motors from below (Fig. 1). During experiment, the vessel was filled with water to height level H_0 above the plate before setting the plate in motion. Food colouring was added to accentuate the water and a marking was made on the rotating plate to measure its angular velocity and ensure that it was constant.

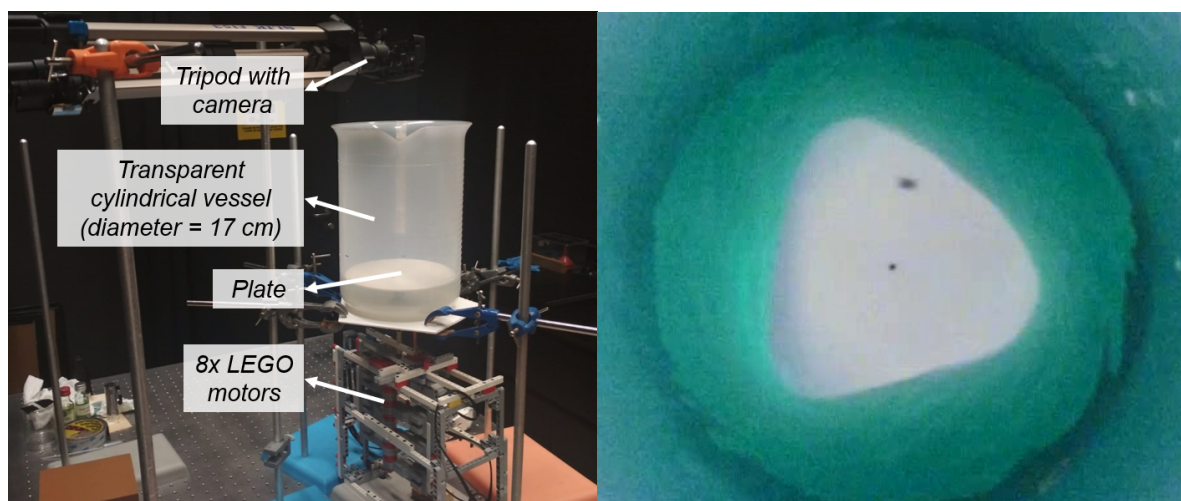


Fig. 1: Experimental setup (left), and view of the camera from above (right).

3 Force Analysis

It was observed experimentally that even though rotational symmetry was broken when a polygon was formed, the height level of fluid at the walls of the vessel remained uniform, i.e. independent of the azimuthal angle. The following analysis will rely heavily on this fact.

I. Qualitative Account

Consider the bottom-most layer of fluid that lies on the plate. Because of the uniform fluid height at the vessel's walls, the pressure difference between a point on the central dry region and a point contacting the walls (both points residing on this layer) is uniform. For a fluid particle travelling along the boundary of the dry region, this pressure difference imparts a radially inward force to it. The magnitude of this force is positively related to the pressure gradient (the rate of change of pressure over distance) between the dry region and the vessel's wall.

In the axisymmetric case, the pressure gradient is just right, such that the resultant force on the particle exactly provides its centripetal force (Fig. 2a). Now consider a small radially inward perturbation to the dry region. The distance between the dry region and the walls increases, whilst the pressure difference remains constant (because the pressure difference is independent of the azimuthal angle), causing the pressure gradient to decrease. As such, the force due to pressure gradient is no longer sufficient to provide the required centripetal force, so the particle accelerates outward in the next instant (Fig. 2b). At this next instant, the distance between the dry region and the walls is now smaller, and pressure difference is still unchanged, so the pressure gradient increases. The force from the pressure gradient is now larger than the required centripetal force, leading to inward motion of the particle at the next instant (Fig. 2c). This leads to a cycle of oscillating pressure gradients which results in the oscillatory motion of the fluid particle. This oscillates the boundary of the dry region, giving rise to polygonal shapes (Fig. 2d).

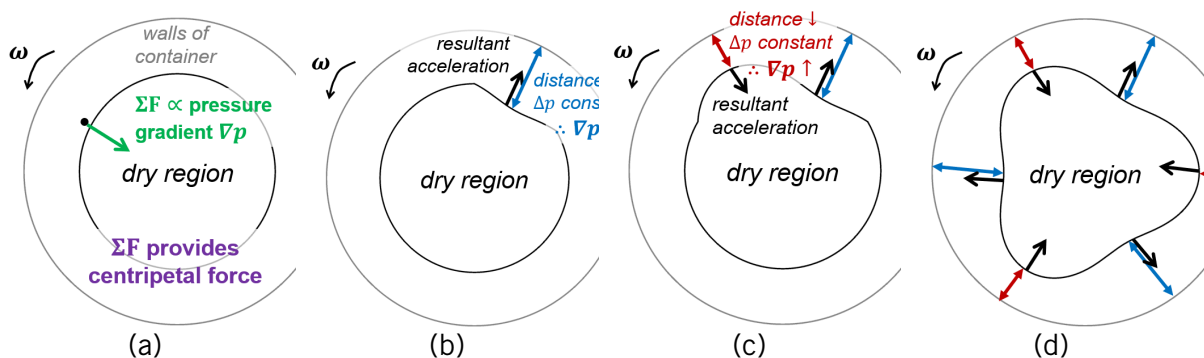


Fig. 2: A fluid particle on the boundary of the dry region tends to exhibit oscillatory motion, such that a small radial perturbation from an initially axisymmetric state [in (a)] eventually causes the dry region to transition from a circle to a polygon [(b)-(d)].

This force approach provides a physical explanation of how the polygons form. It also provides an understanding of how the properties of the polygons vary with parameters, which will be analysed later.

II. Axisymmetric State

Before investigating the asymmetric state where a polygon is formed, we firstly study the axially symmetric state where the dry region is circular. A cylindrical coordinate system is chosen with the reference plane lying along the plate and z -axis passing through the central axis of the plate. In the axisymmetric state where the dry region is circular, fluid flow is only directed in the azimuthal direction and is irrotational (Bergmann et al., 2011), such that the azimuthal velocity U_θ is given by (1).

$$U_\theta = \frac{\Gamma}{2\pi r} \quad (1)$$

where Γ is the circulation of the flow. A relation between Γ and ω can be established in a similar manner to Tophøj et al. (2013); by considering a balance of torques between the driving torque from the plate and the resistive torque arising from skin friction with the vessel walls. Further details are in Appendix A.

III. Asymmetric State

Here we consider the shape of the polygon at the steady state. The boundary of the polygon is described by the curve l , such that the polygon's boundary is given by $r = l(\theta)$, where θ is the azimuthal angle. In the lab reference frame, the polygon rotates at $\Omega < \omega$ in the same direction as the plate. To simplify analysis, we take on the reference frame that rotates at Ω along with the polygon, so that the polygon appears stationary in our frame. Let us consider a slice of fluid at azimuthal angle θ , and the variation of the height of the fluid surface along this slice with radial distance, $h(r)$. Fig. 3 shows a possible plot of $h(r)$, and the forces acting on a specific particle that lies on the fluid surface of this slice at radial distance r . $\omega'(r)$ is defined as the angular velocity of this surface particle (in the rotating frame).

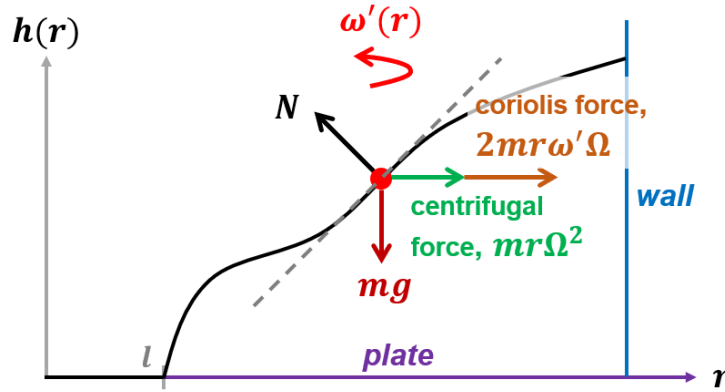


Fig. 3: Sketch of a possible $h(r)$, starting from $r = l$, the boundary of the polygon (which is dependent on θ), and ending at $r = R$, the wall. Forces on a surface particle located at radial distance r include its weight, normal force (from the rest of the fluid), centrifugal and Coriolis forces that arise from the rotating frame.

Under the assumption that the length scale of vertical oscillations is small compared to that of horizontal oscillations, $\Sigma F_y \approx 0$. Writing Newton's Second Law in the radial direction, a general equation of motion can be derived for any particle on the surface as shown in (2).

$$\frac{d^2r}{dt^2} = r(\Omega + \omega')^2 - g \frac{dh}{dr} \quad (2)$$

ω' is generally not known for most of the fluid particles, as fluid flow in this asymmetric state is very complex in nature. However, ω' is known for some "special" particles. Since fluid flow at the boundary layers between the fluid body and solid surfaces are dominated by viscous effects, ω' of particles at the fluid-plate and fluid-wall boundary layers are expected to retain their original ω' from the axisymmetric state. As such, for the surface particle at $r = l$, i.e. the boundary of the polygon, $\omega' = \frac{\Gamma}{2\pi l^2} - \Omega$. Applying this to (2) produces a differential equation for $l(\theta)$, in (3):

$$\frac{d^2l}{d\theta^2} = \left(\frac{\Gamma}{2\pi l^2} - \Omega \right)^2 \frac{d^2l}{d\theta^2} - \frac{\Gamma}{\pi l^3} \left(\frac{\Gamma}{2\pi l^2} - \Omega \right) \left(\frac{dl}{d\theta} \right)^2 = \frac{\Gamma^2}{4\pi^2 l^3} - g \frac{dh}{dr} \Big|_{r=l} \quad (3)$$

To deduce the final term in (3), the mathematical form of $h(r)$ needs to be investigated. A few conditions about $h(r)$ are known: it starts at zero at $r = l$, giving (4); it ends at some uniform height at the wall $r = R$, giving (5). For the surface particle at the wall where $r = R$, $\omega' = \frac{\Gamma}{2\pi R^2} - \Omega$ since it is part of the fluid-wall boundary layer, so applying (2) to this particle gives a constraint for its gradient in (6). Finally, a constraint on the total fluid volume present in the setup produces (7).

$$h(l) = 0 \quad (4)$$

$$h(R) = H \quad (5)$$

$$h'(R) = \frac{\Gamma^2}{4g\pi^2 R^3} \quad (6)$$

$$\int_l^R r h(r) dr = \frac{1}{2} R^2 H_0 \quad (7)$$

From these four conditions, $h(r)$ can be reasonably approximated to take on a cubic polynomial form. The differential equation from (3) can now be completed to yield (8), which can be numerically solved.

$$= \frac{\Gamma^2}{4\pi^2 l^3} - g \left[\frac{\left(\frac{\Gamma}{2\pi l^2} - \Omega\right)^2 \frac{d^2 l}{d\theta^2} - \frac{\Gamma}{\pi l^3} \left(\frac{\Gamma}{2\pi l^2} - \Omega\right) \left(\frac{dl}{d\theta}\right)^2}{(l-R)^2(3l+2R)} + \frac{\Gamma^2(2l+3R)}{4g\pi^2 R^3(3l+2R)} \right] \quad (8)$$

4 Results and Discussion

I. Height Profile

The cubic form for $h(r)$ generally produces curves similar to Fig. 4a, which start out concave and end off convex. Experimentally, by shining high-intensity light onto a slice of fluid from above, the surface of the fluid slice was illuminated, and its side view image is shown in Fig. 4b. There is a good agreement, between theory and experiment, in the general shapes of the fluid surface profiles.

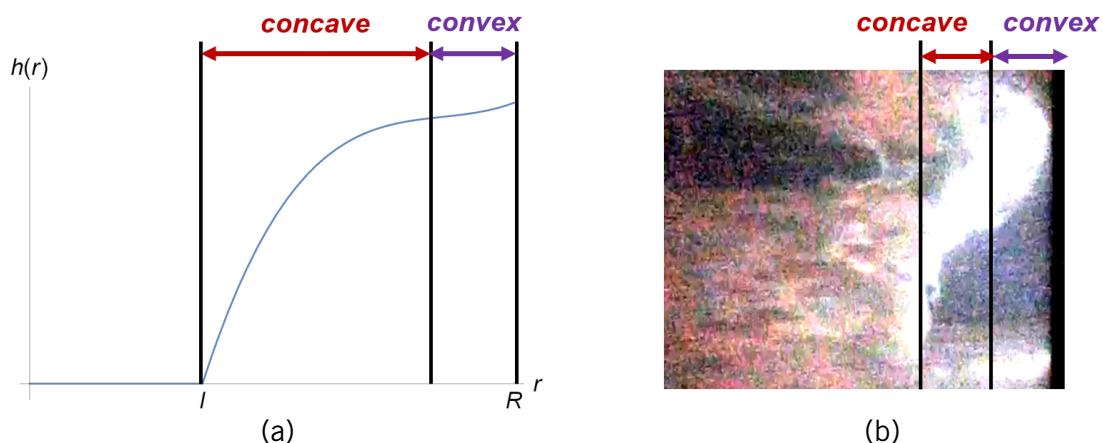


Fig. 4: (a) Example of theoretical height profile $h(r)$, and (b) experimentally captured height profile.

II. Polygon Shape

For sufficiently large H_0 and ω , the dry region was found to produce elliptical shapes (Fig. 5a). Triangles were formed when ω was further increased (Fig. 5b). This trend agrees with what was found by Jansson et al. (2006). Moreover, the mean radius of the dry region increased with ω .

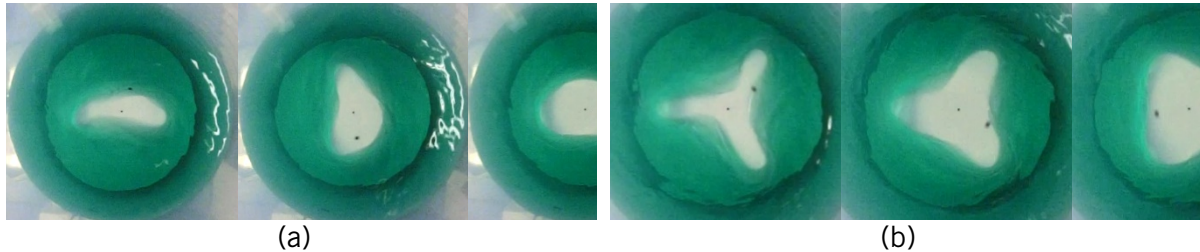


Fig. 5: Experimentally obtained polygons for (a) ellipses, and (b) triangles. Pictures are arranged in sequence of increasing ω .

The previous qualitative account can explain the trend of mean radius increasing with ω . For higher ω , the required centripetal force for a fluid particle travelling along the polygon's boundary increases. The net radially inward force on the particle must therefore increase, which can only be provided by having a steeper pressure gradient. This can only happen provided the distance between the boundary of the dry region and the vessel's walls decreases, which simultaneously increases the dry region's mean radius. Additionally, to explain why the formed polygons have more sides with increasing ω (from $n = 2$ for ellipse to $n = 3$ for triangle), notice that a particle travelling along the boundary of the dry region has less time to experience the force from the pressure gradient for larger ω . The change in velocity of the particle as it passes by the corner of the polygon is hence reduced, so the particle's velocity vector only turns through a smaller angle, resulting in an increase in number of sides of the polygon.

The differential equation in (8) that governs $l(\theta)$ also offered accurate predictive power into the polygon's geometry, as demonstrated in Fig. 6.

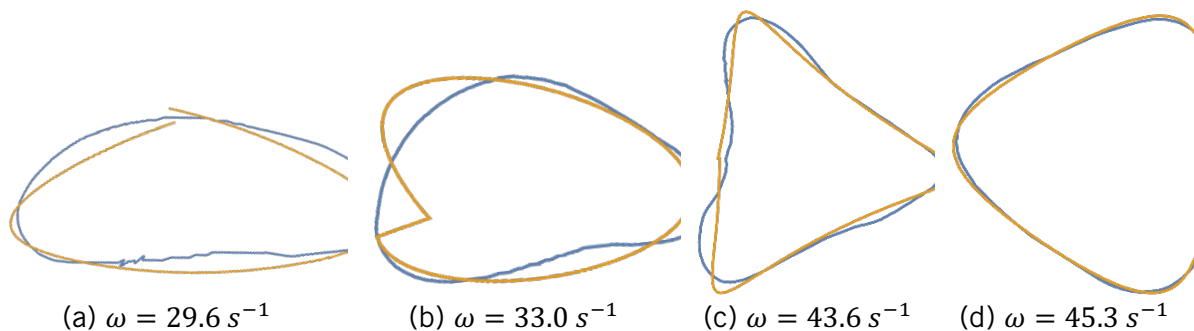


Fig. 6: Shapes of ellipses [in (a) and (b)] and triangles [in (c) and (d)] from experiment (blue) and theory (orange), for varying ω and constant $H_0 = 3.7\text{cm}$. The diagrams are not drawn to scale.

5 Conclusion

Despite the difficulties in attaining the full fluid flow profile in the asymmetric state, this study offered novel theoretical insight into the phenomenon. By using a more indirect and simplified approach concerning the forces on the fluid surface particles, the polygon formation was qualitatively explained, and a single equation governing approximately the polygon's geometry was formulated. This model achieved a high degree of predictive power

into the shape of the polygon formed at the steady state, which closely matched experimental results.

Investigation of higher-order polygons beyond triangles were excluded from this study because owing to the small R of the vessel used, squares and pentagons could only be obtained at higher ω ; but at such high ω , the fluid flow became turbulent and free-surface fluctuations were dominant to the extent that obtained shapes were not stable.

6 Acknowledgements

I am thankful to my teacher mentor Mr Samuel Tan from Hwa Chong Institution, as well as the school lab staff, for providing me with assistance in my experimental setup.

References

1. Jansson, T., Haspang, M., Jensen, K., Hersen, P., & Bohr, T. (2006). Polygons on a Rotating Fluid Surface. *Physical Review Letters*, 96(17). <https://doi.org/10.1103/physrevlett.96.174502>
2. Bergmann, R., Tophøj, L., Homan, T., Hersen, P., Andersen, A., & Bohr, T. (2011). Polygon formation and surface flow on a rotating fluid surface. *Journal Of Fluid Mechanics*, 679, 415-431. <https://doi.org/10.1017/jfm.2011.152>
3. Tophøj, L., Mougel, J., Bohr, T., & Fabre, D. (2013). Rotating Polygon Instability of a Swirling Free Surface Flow. *Physical Review Letters*, 110(19). <https://doi.org/10.1103/physrevlett.110.194502>

Appendix A: Axisymmetric Flow Profile

The full Navier-Stokes equation is written in (9), where $\vec{U}(r, \theta, z)$ denotes the velocity flow field and $P(r, \theta, z)$ describes the fluid pressure.

$$\frac{\partial \vec{U}}{\partial t} + (\vec{U} \cdot \nabla) \vec{U} = -\frac{1}{\rho} \nabla P + \nu \nabla^2 \vec{U} + \vec{g} \quad (9)$$

We are only concerned with the flow profile at the steady state, so we can eliminate time dependence from the equation. In the axially symmetric state, the variables should be independent of θ , and we may assume that secondary flows in the radial and axial directions are non-existent. These simplifications reduce the equation to the form in (10).

$$\frac{U_\theta}{r^2} = \frac{1}{r} \frac{\partial U_\theta}{\partial r} + \frac{\partial^2 U_\theta}{\partial r^2} + \frac{\partial^2 U_\theta}{\partial z^2} \quad (10)$$

Solving for U_θ produces two solutions: $U_\theta \propto r$, which corresponds to solid body rotation, and $U_\theta \propto \frac{1}{r}$, which corresponds to irrotational flow. The former predicts a convex-shaped surface, while the latter predicts a concave-shaped surface. In order to determine which of these solutions corresponds to reality, the fluid height profile in the axisymmetric state is observed experimentally as shown in Fig. 7, and found to be concave. Therefore, the irrotational flow profile is used, in agreement with the findings by Bergmann et al. (2011).



Fig. 7: Side view of the fluid surface in the axisymmetric state, with the fluid surface traced by the red curves.

To determine the relation between Γ and ω , we consider two torques acting on the entire fluid body: τ_d is the torque delivered by the rotating plate, while τ_w is the resistive torque from the walls. At the steady state, these two torques must equate. Both torques can be computed by integrating the shear stress $\sigma(r)$ across each surface, as shown in (11).

$$\tau = \int_{surface} r \sigma(r) dA \quad (11)$$

This shear stress arises from skin friction, which is dependent on the skin friction coefficient C_f of the surface, and the relative velocity between the fluid body and the surface v , in (12).

$$\sigma(r) = \frac{1}{2} C_f \rho v^2 \quad (12)$$

Performing the integration using (11) and (12), and balancing τ_d and τ_w produces a relation between Γ and ω . The relation is also dependent on the ratio of the skin friction coefficient of the wall C_w to that of the plate C_d (since the surfaces of the plate and the walls differ, their skin friction coefficients are also different). This ratio can be determined by fitting with the experimentally determined graph of radius of dry circular region a against ω . Mathematically, a and ω are related by (13).

$$\frac{C_w}{C_d} \left[\frac{\omega^2}{5(R^5 - a^5)} + \frac{2aR\omega(a^3 - R^3)}{3\sqrt{R^2 - a^2 - 2a^2 \ln\left(\frac{R}{a}\right)}} - \frac{2a^2 g H_0 R^2 (a - R)}{R^2 - a^2 - 2a^2 \ln\left(\frac{R}{a}\right)} \right] = \frac{2a^2 g H_0^2 R (R^2 - a^2)}{\left[R^2 - a^2 + 2a^2 \ln\left(\frac{R}{a}\right) \right]^2} \quad (13)$$

The best fit for the graph of a against ω is obtained for a C_w/C_d ratio of 1.8, as shown in Fig. 8.

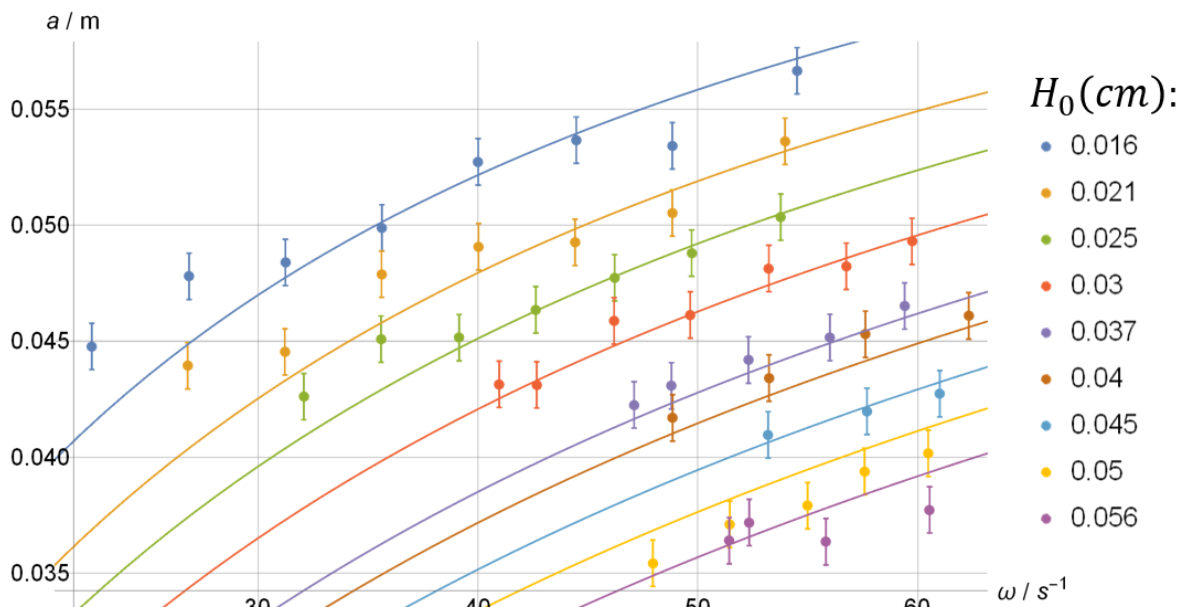


Fig. 8: Experimentally determined a for different values of ω and H_0 shown by the plot points, and the theoretical curves produced for the best-fit C_w/C_d ratio.

This best-fit ratio of skin friction coefficients is used in the relation between Γ and ω , which is used in the rest of the theoretical model.